

The effect of wind shear and curvature on the gravity wave drag produced by a ridge

Article

Accepted Version

Teixeira, M. A. C. ORCID: <https://orcid.org/0000-0003-1205-3233> and Miranda, P. M. A. (2004) The effect of wind shear and curvature on the gravity wave drag produced by a ridge. *Journal of the Atmospheric Sciences*, 61 (21). pp. 2638-2643. ISSN 1520-0469 doi: <https://doi.org/10.1175/JAS3282.1>
Available at <https://centaur.reading.ac.uk/29253/>

It is advisable to refer to the publisher's version if you intend to cite from the work. See [Guidance on citing](#).

To link to this article DOI: <http://dx.doi.org/10.1175/JAS3282.1>

Publisher: American Meteorological Society

All outputs in CentAUR are protected by Intellectual Property Rights law, including copyright law. Copyright and IPR is retained by the creators or other copyright holders. Terms and conditions for use of this material are defined in the [End User Agreement](#).

www.reading.ac.uk/centaur

CentAUR

Central Archive at the University of Reading

Reading's research outputs online



The Effect of Wind Shear and Curvature on the Gravity Wave Drag Produced by a Ridge

MIGUEL A. C. TEIXEIRA AND PEDRO M. A. MIRANDA

Centro de Geofísica, and Department of Physics, University of Lisbon, Lisbon, Portugal

(Manuscript received 8 January 2004, in final form 22 April 2004)

ABSTRACT

The analytical model proposed by Teixeira, Miranda, and Valente is modified to calculate the gravity wave drag exerted by a stratified flow over a 2D mountain ridge. The drag is found to be more strongly affected by the vertical variation of the background velocity than for an axisymmetric mountain. In the hydrostatic approximation, the corrections to the drag due to this effect do not depend on the detailed shape of the ridge as long as this is exactly 2D. Besides the drag, all the perturbed quantities of the flow at the surface, including the pressure, may be calculated analytically.

1. Introduction

Recently, Teixeira et al. (2004) presented a linear model of mountain waves for wind profiles with shear and curvature based on the Wentzel–Kramers–Brillouin (WKB) approximation. This model provided new analytical expressions for the wave drag as a function of the first and second derivatives of the background velocity profile. These expressions were shown to be asymptotically in agreement with previously known exact formulas, and to reproduce to a good degree of approximation the results of numerical mesoscale simulations for similar input conditions. They were able to elucidate, in particular, why two flows that turn with height in different ways lead to opposite dependencies of the drag on the Richardson number.

Teixeira et al. (2004) considered the drag of hydrostatic flow over an isolated axisymmetric mountain. Two-dimensional (2D) orography is also frequently used in idealized studies of mountain waves, since it roughly approximates elongated ridges, which are common in nature. It is therefore of great practical interest to study the drag on this type of orography, for which the equations of motion simplify considerably due to symmetry. In this paper, the model of Teixeira et al. (2004) is extended to calculate the gravity wave drag associated with hydrostatic flow over an isolated 2D ridge.

The property that the corrections to the drag due to the variation of the wind with height are independent of the detailed shape of the orography is shown to also

hold in the present case. However, the coefficients of these corrections are different from the axisymmetric case, due to the different geometry of the problem. Furthermore, in the case of a bell-shaped ridge (and presumably also for other simple types of orography), the perturbations of the flow variables at the surface may be calculated analytically.

2. Model equations

Consider a stably stratified flow over an infinite isolated 2D mountain ridge. If a reference frame is defined such that the ridge is aligned in the y direction, and the background state of the atmosphere is horizontally uniform, the perturbations associated with the internal gravity waves generated by this orography are independent of y . If the fundamental equations of motion with the Boussinesq approximation are linearized with respect to these perturbations (which can be done if they are sufficiently small), and the perturbations are expressed as Fourier integrals along x , an equation may be derived for the vertical structure of \hat{w} , the Fourier transform of the vertical velocity perturbation. This is the Taylor–Goldstein equation (Nappo 2002):

$$\hat{w}'' + \left(\frac{N^2}{U^2} - \frac{U''}{U} \right) \hat{w} = 0. \quad (1)$$

Here, N is the Brunt–Väisälä frequency (assumed constant), U is the background velocity (along x) and the primes denote differentiation along the vertical direction z . This equation was obtained by additionally assuming that the flow is steady and hydrostatic. The linear and hydrostatic approximations, although valid simultaneously only for very gentle orography, enable one to

Corresponding author address: Miguel A. C. Teixeira, Centro de Geofísica da Universidade de Lisboa, Edifício C8, Campo Grande, 1749-016 Lisbon, Portugal.
E-mail: mateixeira@fc.ul.pt

isolate the effects that are the focus of this study from nonlinear and nonhydrostatic effects. Compared with Eq. (13) of Teixeira et al. (2004), (1) is simplified by the symmetry along y , which means that the y component of the horizontal wavenumber vector $\mathbf{k} = (k_1, k_2)$ is $k_2 = 0$. For that reason, the horizontal wavenumber will be called simply k .

As is well known, when the coefficient multiplying \hat{w} in (1) varies relatively slowly with z , this equation may be solved using the WKB approximation. Following Teixeira et al. (2004), the approximate WKB solution of (1) valid up to second-order in the small perturbation parameter ε is

$$\hat{w} = \hat{w}(z = 0) \exp \left\{ i \int_0^z [m_0(\varepsilon z') + \varepsilon m_1(\varepsilon z') + \varepsilon^2 m_2(\varepsilon z')] dz' \right\}, \quad (2)$$

where m_0 , m_1 , and m_2 are the zeroth-, first-, and second-order coefficients of the series expansion of the vertical wavenumber of the internal gravity waves in powers of ε .

When introduced into (1), the solution (2) yields the following definitions:

$$m_0 = \frac{N}{U} \operatorname{sgn}(k), \quad (3)$$

$$\varepsilon m_1 = -\frac{i}{2} \frac{U'}{U}, \quad (4)$$

$$\varepsilon^2 m_2 = -\frac{1}{8} \frac{U}{N} \operatorname{sgn}(k) \left(\frac{U'^2}{U^2} + 2 \frac{U''}{U} \right). \quad (5)$$

In (3)–(5), the radiation boundary condition at $z \rightarrow +\infty$ is implicitly assumed, since the sign of m_0 and m_2 is the same as that of k , implying upward energy propagation. These expressions are analogous to Eqs. (22)–(24) of Teixeira et al. (2004), but simplified for 2D, hydrostatic flow. With the addition of the boundary condition at the surface,

$$\hat{w}(z = 0) = iU_0 k \hat{\eta}, \quad (6)$$

the solution to the problem is fully specified. Here, $\hat{\eta}$ is the Fourier transform of the surface elevation, and U_0 is the background velocity at the surface.

3. Mountain wave drag

For a 2D mountain ridge, the total gravity wave drag, defined as the area integral of the pressure perturbation times the gradient of the ground elevation, is infinite, because the ridge is itself infinite along y , and it only makes sense to define a drag per unit length in the transverse direction. In the linear approximation, this is given by

$$D = \int_{-\infty}^{+\infty} p(z = 0) \frac{\partial \eta}{\partial x} dx, \quad (7)$$

where p is the pressure and η is the surface elevation. The drag can also be calculated in Fourier space, through the integral

$$D = 2\pi i \int_{-\infty}^{+\infty} k \hat{p}^*(z = 0) \hat{\eta} dk, \quad (8)$$

where \hat{p}^* is the complex conjugate of the Fourier transform of the pressure. In the present approximation, $\hat{p}(z = 0)$ is given by

$$\hat{p}(z = 0) = i\rho_0 U_0^2 \left[m_0(z = 0) + \varepsilon m_1(z = 0) + i \frac{U'_0}{U_0} + \varepsilon^2 m_2(z = 0) \right] \hat{\eta}, \quad (9)$$

where ρ_0 is the reference density of air [cf. Eq. (31) of Teixeira et al. 2004]. Using the results (3)–(5), (9) becomes

$$\hat{p}(z = 0) = i\rho_0 N U_0 \left[\operatorname{sgn}(k) + \frac{i}{2} \frac{U'_0}{N} - \frac{1}{8} \operatorname{sgn}(k) \left(\frac{U_0'^2}{N^2} + 2 \frac{U_0 U_0''}{N^2} \right) \right] \hat{\eta}, \quad (10)$$

where U_0' and U_0'' are the first and second derivatives of the background velocity at the surface. Introducing the complex conjugate of this equation into (8), the drag may be written

$$D = 2\pi\rho_0 N U_0 \left(1 - \frac{1}{8} \frac{U_0'^2}{N^2} - \frac{1}{4} \frac{U_0 U_0''}{N^2} \right) \times \int_{-\infty}^{+\infty} |k| |\hat{\eta}|^2 dk. \quad (11)$$

In (11), $|k|$ appears inside the integral because of the $\operatorname{sign}(k)$ factor in the terms of zeroth and second order in ε of the pressure perturbation \hat{p} . The part of the drag corresponding to the first-order term cancels, because the $\operatorname{sign}(k)$ factor is absent. Since $|\hat{\eta}|^2$ is even when the surface elevation function $\eta(x)$ is real, this part of the integral is zero, because the corresponding integrand is odd.

Noting that, by (11), the drag in the absence of shear is defined as

$$D_0 = 2\pi\rho_0 N U_0 \int_{-\infty}^{+\infty} |k| |\hat{\eta}|^2 dk, \quad (12)$$

the drag for the general case may be expressed more compactly as

$$D = D_0 \left(1 - \frac{1}{8} \frac{U_0'^2}{N^2} - \frac{1}{4} \frac{U_0 U_0''}{N^2} \right). \quad (13)$$

It is clear that the corrections to the drag due to shear and curvature of the background wind profile do not depend on the form of the function $\hat{\eta}$ (note that the hydrostatic assumption is essential for this property to be verified). This equation, which is analogous to Eqs. (50)–(51) of Teixeira et al. (2004), is nevertheless much shorter, due to the simplifications brought by the 2D geometry.

The drag given by (13) is per unit length and so cannot be directly compared with the drag calculated by Teixeira et al. (2004), but the relative corrections due to the shear and curvature of the wind profile, put in evidence by (13), are of a similar nature and may be compared. These corrections differ from those valid for an axisymmetric mountain, with the 1/8 and 1/4 coefficients, multiplying, respectively, $U_0'^2/N^2$ and $U_0 U_0''/N^2$ in (13), being larger by a factor of 4/3. This means that the effect on the drag of the shear and curvature of the wind profile is qualitatively similar, but stronger for 2D than for 3D flow.

For a linear wind profile of the form

$$U = U_0 \left(1 - \frac{z}{z_c} \right), \quad (14)$$

where z_c is constant, (13) reduces to

$$D = D_0 \left(1 - \frac{1}{8\text{Ri}} \right), \quad (15)$$

where $\text{Ri} = N^2/U_0'^2 = N^2 z_c^2/U_0^2$ is the Richardson number of the flow. This expression may be compared with the corresponding result obtained analytically by Smith (1986) for a linear profile with an arbitrarily large shear rate. It may be shown that, in the present notation, Smith's drag expression [his Eq. (3.17)] is

$$D = D_0 \left(1 - \frac{1}{4\text{Ri}} \right)^{1/2}, \quad (16)$$

and it is straightforward to show that both expressions are asymptotically equal in the limit of large Ri. The consistency of the two approaches, which parallels the asymptotic agreement found between the 3D model of Teixeira et al. (2004) and the exact drag expression of Grubišić and Smolarkiewicz (1997), gives further confidence in the WKB approach adopted here.

Figure 1a shows a comparison between the normalized drag given by (15) and data taken from the mesoscale, nonhydrostatic numerical model NH3D (Miranda and James 1992). This model is 3D, but was run here for a 2D ridge using a sufficiently wide domain of integration. The domain comprises $65 \times 65 \times 120$ grid points, and the conditions considered in the runs were very approximately linear and hydrostatic ($Nh/U_0 = 0.01$ and $Na/U_0 = 23$, where h is the maximum height

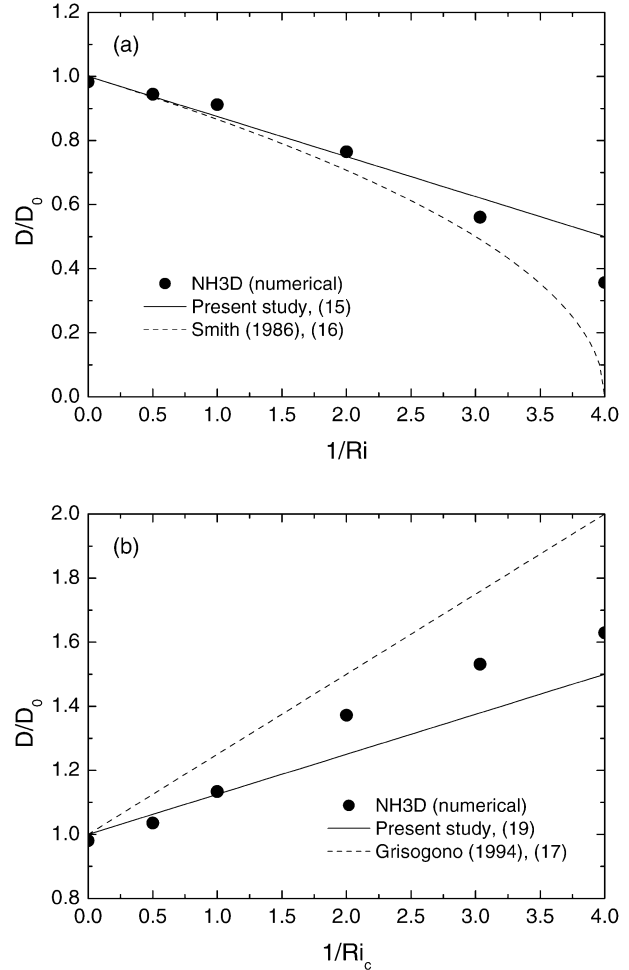


FIG. 1. Normalized drag as a function of the inverse Richardson number. (a) Linear background velocity profile (14). (b) Parabolic background velocity profile (18). The NH3D model uses $Na/U_0 = 23$, $Nh/U_0 = 0.01$.

of the ridge and a is its half width), in order to isolate the effect of shear. Also shown is the drag given by Smith's expression (16). It may be seen that the agreement with (15) is nearly as good as with (16). However, the value taken by D/D_0 at $\text{Ri} = 1/4$ is larger than zero, in contradiction with what is predicted by (16). Since, for this value of Ri, the flow should be close to becoming hydrodynamically unstable, neither analytical result is formally accurate, and this is perhaps why the numerical results are not closer to the exact formula of Smith (1986).

When the wind profile is more complicated than (14), both shear and curvature terms are important in (13). An early attempt to evaluate the effect of the curvature of the wind profile on the surface drag on a 2D ridge using a WKB approximation was made by Grisogono (1994). In the present notation, and for inviscid conditions, Grisogono's drag expression [his Eq. (4.8)] reads

$$D = D_0 \left(1 - \frac{1}{2} \frac{U_0 U_0''}{N^2} \right). \quad (17)$$

The coefficient multiplying the curvature term is larger by a factor of 2 than that present in (13) and the term proportional to $U_0'^2$ is absent. The reasons for these discrepancies have to do with an inconsistent application of the WKB method and are discussed in detail by Teixeira et al. (2004).

When studying the effect of curvature of the wind profile on mountain wave drag in 2D, it is not possible to consider a flow simultaneously with a constant N and a constant Richardson number, as was done for the 3D situation by Teixeira et al. (2004). So, the simplest flow with nonzero second derivative, a parabolic wind profile, is considered next:

$$U = U_0 \left[1 - \left(\frac{z}{z_c} \right)^2 \right]. \quad (18)$$

In this flow $U_0' = 0$, hence the Richardson number at the surface is infinite. However, the curvature is $U_0'' = -2U_0/z_c^2$, and this can be related to the Richardson number at the critical level ($z = z_c$), $Ri_c = N^2 z_c^2 / 4U_0^2$, which is the important parameter for this flow. [Note that Ri in the previous flow (14) is also the Richardson number at the critical level.] It turns out that the drag expression (13) reduces in this case to

$$D = D_0 \left(1 + \frac{1}{8Ri_c} \right). \quad (19)$$

So, the drag increases as Ri_c decreases, unlike the previous case, despite the qualitative similarity of the background wind profiles (14) and (18).

In Fig. 1b, the drag calculated with (19) is compared with data from numerical simulations of the NH3D model for approximately linear and hydrostatic conditions ($Nh/U_0 = 0.01$ and $Na/U_0 = 23$). Also shown is the prediction from Grisogono's formula (17). It is clear that the prediction of (19) is not as good as in the previous case, with some drag underestimation, especially at relatively low Ri_c . This resembles the behavior of the drag for a turning wind over an axisymmetric mountain in Fig. 7 of Teixeira et al. (2004), where the curvature is also negative at the surface. Nevertheless, qualitatively, and in order-of-magnitude terms, the agreement is satisfactory. Curiously, (17) gives a better prediction of the drag than expected, but is clearly inferior to (19), especially for large Ri_c .

4. The surface pressure perturbation

In order to understand the behavior of the drag, it is useful to calculate the surface pressure perturbation (as was done in 3D by Teixeira et al. 2004). In fact, at the surface, it is straightforward to calculate not only the pressure but also all other relevant variables of the flow.

However, some of them, such as the vertical velocity perturbation, the buoyancy perturbation b , and the spanwise velocity perturbation v , are related in a trivial way to the surface elevation η . Apart from the pressure, the only other variable of the flow that is affected at the surface by the vertical variation of the background velocity is the streamwise velocity perturbation u (which is relevant for downslope windstorms).

Note that $p(z = 0)$ may be obtained by calculating the inverse Fourier transform of (10). Although the only expressions depending on k in (10) are $\text{sign}(k)$ and $\hat{\eta}$, and this renders the integration analytical in most cases, the presence of $\text{sign}(k)$ means that $\hat{\eta}$ must be specified. Here, an isolated bell-shaped ridge will be used as an example. The corresponding Fourier transform is

$$\hat{\eta} = \frac{1}{2} h a e^{-a|k|}. \quad (20)$$

Then, it is found from (10) that

$$\begin{aligned} \frac{p(z=0)}{\rho_0 N U_0 h} = & - \left(1 - \frac{1}{8} \frac{U_0'^2}{N^2} - \frac{1}{4} \frac{U_0 U_0''}{N^2} \right) \frac{x/a}{1 + (x/a)^2} \\ & - \frac{1}{2} \frac{U_0'}{N} \frac{1}{1 + (x/a)^2}. \end{aligned} \quad (21)$$

The pressure perturbation thus comprises two parts: the first one, which is antisymmetric with respect to the ridge, produces drag; the second one, which is symmetric, and in fact proportional to the surface elevation, does not produce drag.

Figure 2a shows the pressure perturbation as a function of streamwise distance for different values of Ri for the linear background velocity profile (14). The continuous lines correspond to (21), while the symbols represent output from the NH3D numerical model for the same conditions as considered in Fig. 1a. For high Ri , the pressure distribution tends to be antisymmetric with respect to the orography, in agreement with the linear theory of Queney (see Smith 1979). As Ri decreases, the antisymmetric component of the pressure perturbation weakens and the symmetric component becomes more prominent. The analytical expression reproduces the numerical simulation data quite accurately, except for $Ri = 0.25$, confirming that the WKB approximation can be used for Ri as low as 0.5 (as happened in the 3D case). Of course, this is also consistent with the behavior of the drag in Fig. 1a.

Figure 2b presents the pressure perturbation for the parabolic background velocity profile (18). In this case $U_0' = 0$, and hence, according to (21), the symmetric component of the pressure vanishes. The pressure perturbation is thus predicted to be perfectly antisymmetric. When the analytical results given by (21) are compared with the numerical results, this aspect is confirmed, except for $Ri_c = 0.25$, and to a much lesser degree for $Ri_c = 0.5$. However, the magnitude of the pressure is considerably underestimated by the analytical model for

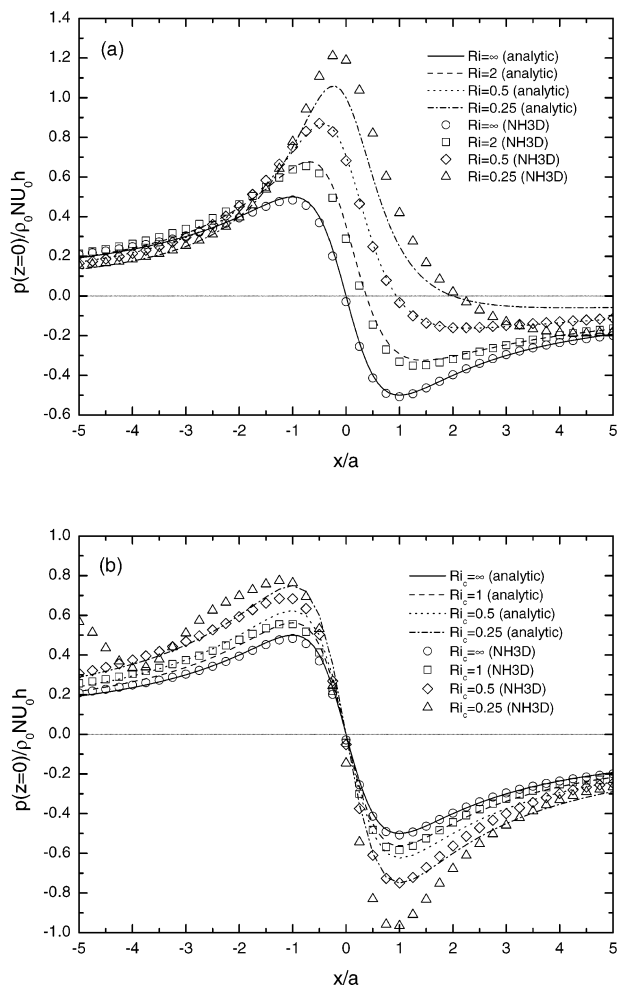


FIG. 2. Normalized pressure perturbation at $z = 0$ as a function of normalized streamwise distance for the same conditions as Fig. 1. (a) Linear background velocity profile (14). (b) Parabolic background velocity profile (18). Analytic results are calculated from (21).

$Ri_c < 1$. This is consistent with the worse prediction of the drag, when compared with the previous case, for similar values of Ri .

Especially for the linear background velocity profile, the pressure perturbation given by the NH3D model tended to drift slightly in time, so as to appear in the plots translated vertically upward or downward by a constant when compared with the analytical result, although its shape was in close agreement. This feature, which is related to imperfections in the implementation of the boundary conditions in the numerical model, has been corrected by subtracting from the pressure perturbation given by NH3D the integral of the pressure over the domain,

$$\int_{-L}^L \frac{p(z=0)}{\rho_0 N U_0 h} d\left(\frac{x}{a}\right), \quad (22)$$

and adding to it the theoretical value of this integral, which from (21) is seen to be

$$\int_{-L}^L \frac{p(z=0)}{\rho_0 N U_0 h} d\left(\frac{x}{a}\right) = -\frac{U'_0}{N} \arctan\left(\frac{L}{a}\right) = -\text{sign}(U'_0) Ri^{-1/2} \arctan\left(\frac{L}{a}\right). \quad (23)$$

In (22) and (23), L is the half width of the domain. Obviously, in these expressions, only the symmetric part of the pressure contributes to the integral of the pressure perturbation so, for the parabolic velocity profile, the integral is zero.

5. Discussion

The calculations carried out in this study might be useful for including the effects of shear and curvature of the wind profile in parameterizations of gravity wave drag for flow over elongated ridges. The independence of the drag expressions derived here from the detailed shape of the ridge is probably more relevant than the corresponding result for axisymmetric orography, since approximately 2D mountains and mountain ranges are relatively common.

As for an axisymmetric mountain, it appears that the drag depends, to a first approximation, on the characteristics of the background flow at the surface. The slightly worse performance of the model for a velocity profile with curvature, which is probably caused by the variation of U and U' with height (an effect that is not accounted for), does not contradict this conclusion.

The effects of shear and curvature of the wind profile are found to be qualitatively similar to those for flow over an axisymmetric mountain (with negative curvature increasing the drag and shear decreasing it), but stronger. This happens because, in flow over a ridge, the air is not deflected laterally, and this causes the vertical wavelength of the internal gravity waves to be larger, making the waves “sample” the shear more deeply—a similar effect can be observed in Fig. 7 of Grubišić and Smolarkiewicz (1997), where the exact results of these authors and of Smith (1986) are compared.

For related reasons, it is necessary to be cautious when extrapolating the present results to large amplitude ridges: nonlinear effects are known to be more important in 2D than in 3D geometries (Miranda and James 1992). In fact, preliminary numerical simulations for higher values of Nh/U_0 (not shown) suggest that the drag increases considerably, probably due to the strong nonlinearity that always exists at the critical level. Nevertheless, the drag retains some of its qualitative behavior for the range of Ri considered here. Outside the scope of this study are, of course, situations where nonlinear or nonhydrostatic effects are overwhelming, such as wave breaking, or wave trapping (Keller 1994).

Acknowledgments. This work was supported by Fundação para a Ciência e Tecnologia (FCT) under Grant SFRH/

BPD/3533/2000 and project BULET/33980/99, cofinanced by the European Union under program FEDER.

REFERENCES

- Grisogono, B., 1994: Dissipation of wave drag in the atmospheric boundary layer. *J. Atmos. Sci.*, **51**, 1237–1243.
- Grubišić, V., and P. K. Smolarkiewicz, 1997: The effect of critical levels on 3D orographic flows: Linear regime. *J. Atmos. Sci.*, **54**, 1943–1960.
- Keller, T. L., 1994: Implications of the hydrostatic assumption on atmospheric gravity waves. *J. Atmos. Sci.*, **51**, 1915–1929.
- Miranda, P. M. A., and I. N. James, 1992: Non-linear three dimensional effects on the wave drag: Splitting flow and breaking waves. *Quart. J. Roy. Meteor. Soc.*, **118**, 1057–1081.
- Nappo, C. J., 2002: *An Introduction to Atmospheric Gravity Waves*. International Geophysics Series, Vol. 85, Academic Press, 276 pp.
- Smith, R. B., 1979: The influence of mountains on the atmosphere. *Advances in Geophysics*, Vol. 21, Academic Press, 87–230.
- , 1986: Further development of a theory of lee cyclogenesis. *J. Atmos. Sci.*, **43**, 1582–1602.
- Teixeira, M. A. C., P. M. A. Miranda, and M. A. Valente, 2004: An analytical model of mountain wave drag for wind profiles with shear and curvature. *J. Atmos. Sci.*, **61**, 1040–1054.